Inorganic Chemistry

Article

pubs.acs.org/IC

Polynuclear Iron(II)–Aminotriazole Spincrossover Complexes (Polymers) In Solution

Irene Bräunlich,[†] Antoni Sánchez-Ferrer,[‡] Matthias Bauer,[§] Rahel Schepper,[§] Philippe Knüsel,[†] Julia Dshemuchadse,[†] Raffaele Mezzenga,[‡] and Walter Caseri*[,†]

[†]Department of Materials, Eidgenössische Technische Hochschule (ETH) Zürich, Wolfgang-Pauli-Strasse 10, 8093 Zürich, Switzerland

[‡]Department of Health Sciences and Technology, Eidgenössische Technische Hochschule (ETH) Zürich, Schmelzbergstrasse 9, 8092 Zürich, Switzerland

[§]Fachbereich Chemie, Technische Universität Kaiserslautern, Erwin-Schrödinger-Strasse, 67663 Kaiserslautern, Germany

Supporting Information

ABSTRACT: Polynuclear spincrossover (SCO) complexes prepared by the combination of $[Fe(DMF)_6]^{2+}$ and NH_2trz (NH_2trz = 4-amino-1,2,4-triazole) were studied ($2ns^-$ = counterion 2-naphthalenesulfonate). It is demonstrated that these $[Fe(NH_2trz)_3](2ns)_2$ complexes can be dissolved—contrary to common reported experience—in *N*,*N*-dimethylformamide (DMF) and, therefore, can be conveniently processed by simple means. The resulting solutions were examined with UV/vis and X-ray absorption spectroscopy (XANES and EXAFS) as well as with small-angle X-ray scattering (SAXS). At a molar NH_2trz/Fe^{2+} ratio of 3/1, corresponding to the stoichiometric ratio of the ideal coordination compound, $[Fe(NH_2trz)_3]^{2+}$ in the low-spin state was found to be in equilibrium with polynuclear species in the high-spin state. The equilibrium can be shifted virtually completely to the side of low-spin Fe^{2+} by an excess of the ligand. The polymer therewith formed contains 100 or more Fe^{2+} ions and is of a pronounced rigid-rod structure, with Fe–Fe distances around 3.32 Å (in comparison to 3.94 Å of the polynuclear species in the high-spin state). Reversible spin crossover takes place in solution upon a temperature increase to around 60 °C; this process is associated with a shift in equilibrium toward species shorter than the initial polynuclear species.

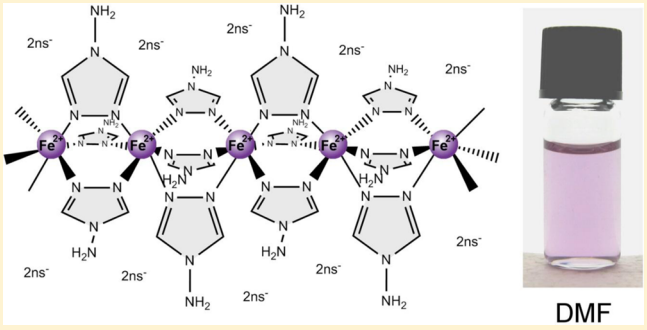

INTRODUCTION

Fe^{2+}-triazole complexes of the general formula $[Fe(Rtrz)_3]X_2$ (Rtrz = 4-R-1,2,4-triazole) belong to the class of polynuclear coordination compounds (polymers). They are characterized by a backbone of linearly arranged Fe^{2+} ions connected by 1,2,4-triazole ligands (Figure 1).[1] The polymeric structures have been substantiated in the case of $[Fe(NH_2trz)_3](NO_3)_2 \cdot xH_2O$ (NH_2trz = 4-amino-1,2,4-triazole) by X-ray diffraction of a single crystal[2] and in other cases by extended X-ray absorption fine structure (EXAFS) analysis[3,4] or infrared (IR) spectroscopy.[5] Some of those complexes have found particular attraction not only for their unusual structures but also for their thermally induced spin crossover (SCO): i.e., reversible switching between low- and high-spin states.[6] Notably, as Fe^{2+} belongs to the d^6 ions, spin crossover is associated with a transition from the diamagnetic to the paramagnetic state and, moreover, is often accompanied by a change in color.

In particular, compounds with the ligand 4-amino-1,2,4-triazole (NH_2trz) have been the focus of many studies in which a variety of counterions have been employed. In comparison to 4-*N*-alkyl-substituted compounds, the mass fraction of iron centers in NH_2trz-based complexes is significantly higher; for example, $[Fe(NH_2trz)_3]Cl_2$ contains 18.1% w/w iron compared to only 5.2% w/w in $[Fe(C_{18}trz)_3]Cl_2$[7] ($C_{18}trz$ = 4-octadecyl-

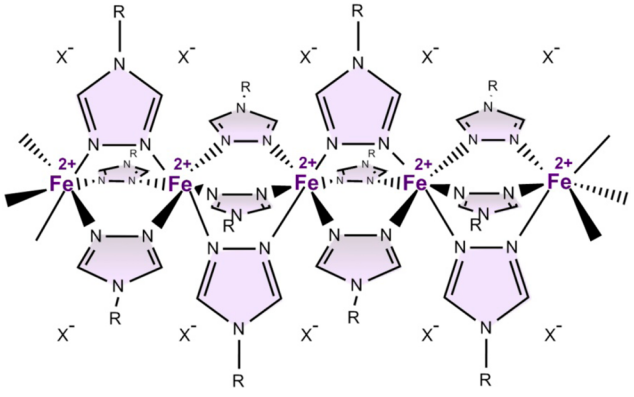

Figure 1. General structure of Fe^{2+} triazole coordination compounds.

Received: December 12, 2013
Published: March 17, 2014

   dx.doi.org/10.1021/ic403035u | *Inorg. Chem.* 2014, 53, 3546–3557

1,2,4-triazole). In addition, alkyl groups are expected to affect in an unfavorable way a number of materials properties of rigid-rod structures (such as $[Fe(Rtrz)_3]X_2$).[8]

The spincrossover temperatures of $[Fe(NH_2trz)_3]X_2$ crucially depend on the counteranions. They have been found to vary between −73 °C (TiF_6^{2-})[9] and 83 °C (SO_4^{2-}),[10] while 2-naphthalenesulfonate (2ns) has been reported to lead to the rare case of spin crossover in the solid state slightly above room temperature:[11] i.e., the magnetic behavior and color of this compound can be switched by gentle heating and cooling. Solid $[Fe(NH_2trz)_3]X_2$ complexes have been investigated with various methods. For instance, the quasi-one-dimensional structure of $[Fe(NH_2trz)_3]X_2$ complexes was established by X-ray diffraction[2,9] and X-ray absorption spectroscopy (XANES and EXAFS).[3,5] The latter technique was helpful also in determining the change in Fe−Fe distances upon transition from the low- to the high-spin state. Further, the role of noncoordinating water molecules has been intensely discussed.[5] In particular, the formation of hydrogen bonds was proposed to enhance interchain connections and to lead to cooperativity among the spincrossover-active iron(II) ions.[12] Moreover, solid $[Fe(NH_2trz)_3]X_2$ complexes were studied with IR spectroscopy, indicating Fe−N stretching vibrations around 305 cm^{-1},[10] and UV/vis spectra revealed d−d transitions around 500 nm.[10] Finally, spincrossover temperatures were evaluated by Mössbauer spectroscopy and magnetic susceptibility measurements,[9,11] as well as by differential scanning calorimetry.[12]

However, we are not aware that appreciable information on $[Fe(NH_2trz)_3]X_2$ solutions is available. Considering the reversible nature of metal−ligand formation, it is unclear if such polynuclear complexes actually exist in solution, due to possible equilibrium reactions with numerous other species such as Fe^{2+} and free NH_2trz, and in the case of their existence if spin crossover is manifested also in the dissolved state. These aspects will be of paramount importance for processing, which essentially has to proceed from solution, as such complexes do not melt prior to decomposition. Hence, this study is devoted to the investigation of such compounds in solution with several analytical methods, by the example of $[Fe(NH_2trz)_3](2ns)_2$. In addition, the preparation of films deposited from solution is also addressed. Note that the designation polynuclear complexes refers to coordination compounds with two or more metal centers: i.e., it includes basically oligomers as well as polymers in terms of macromolecular chemistry (the transition from oligomers to polymers is fluent). In fact, oligomers are likely to occur in the initial stages of polymer formation.

EXPERIMENTAL SECTION

General Considerations. Compounds were purchased from the following companies: sodium 2-naphthalenesulfonate (Na(2ns)) from Alfa Aesar GmbH (Karlsruhe, Germany); iron(II) chloride tetrahydrate and 4-amino-1,2,4-triazole (NH_2trz) from Merck Chemicals (Zug, Switzerland); L-ascorbic acid from Hänseler AG (Herisau, Switzerland); *N*,*N*-dimethylformamide from Sigma-Aldrich (Buchs, Switzerland). Molecular sieve (3 Å, 0.4−0.8 mm beads) was purchased from ABCR GmbH & Co. KG (Karlsruhe, Germany).

Synthesis of Hexaaquairon(II) 2-Naphthalenesulfonate ($[Fe(H_2O)_6](2ns)_2$). The synthesis of this salt was briefly mentioned previously.[11] Iron(II) chloride tetrahydrate (4.32 g, 21.7 mmol) in 10 mL of H_2O was added to a solution of sodium 2-naphthalenesulfonate (10.00 g, 43.4 mmol) in 300 mL of H_2O. Immediately, a white precipitate formed, which was filtered off and washed twice with 150 mL of H_2O. The product was dried in vacuo (0.1 mbar, 24 h). Yield: 10.46 g (18.1 mmol, 83%). Anal. Found (calcd) for $C_{20}H_{26}O_{12}S_2Fe$ (molar mass: 578.40 g·mol^{-1}, calculated values in brackets): C 41.59% (41.53%), H 4.61% (4.53%). Far-infrared (FIR) (in cm^{-1}): 227 (m), 266 (m), 350 (w), 423 (w), 486 (m), 561 (w). Midinfrared (MIR) (in cm^{-1}): 680 (m), 759 (m), 816 (s), 873 (m), 906 (m), 944 (w), 965 (w), 1040 (s), 1097 (m), 1191 (s, broad), 1348 (m), 1505 (m), 1593 (w), 1648 (s), 1672 (w), 2297 (w, broad), 2386 (w, broad), 3060 (w), 3401 (s, broad). Thermogravimetric analysis (TGA): Loss of water at ∼118 °C, maximum decomposition rate at ∼546 °C.

Synthesis of Tris(1-pyrazolyl)methane. Tris(1-pyrazolyl)-methane (tpz) was synthesized according to the literature.[13] The resulting product was recrystallized twice from hot cyclohexane yielding colorless needles. Anal. Found (calcd) for $C_{10}H_{10}N_6$ (molar mass 214.23 g mol^{-1}): C, 56.13 (56.07); H, 4.62 (4.70); N, 38.98 (39.23). Melting temperature: 91 °C. ^1H NMR (acetone-d_6, δ in ppm, J in Hz): 8.71 (s, 1 H), 7.84 (d, 3 H, J = 2.4), 7.61 (d, 3 H, J = 1.7), 6.39 (dd, 3 H, J = 1.7, 2.4). MIR (in cm^{-1}): 755 (s), 799 (s), 837 (m), 929 (w), 970 (w), 1039 (m), 1086 (s), 1205 (m), 1272 (m), 1295 (m), 1319 (s), 1354 (m), 1387 (s), 1428 (m), 1516 (m), 2860 (w), 2926 (w), 2978 (w), 3125 (w).

Synthesis of $[Fe(tpz)_2](2ns)_2$. $[Fe(H_2O)_6](2ns)_2$ (200 mg, 0.346 mmol) and tpz (tris(pyrazolyl)methane, 148 mg, 0.692 mmol) were dissolved in methanol (25 mL) and stirred for 10 min. The solution was thereafter stored for 4 days at −20 °C. During this time dark violet crystals formed, which were filtered off, washed with 20 mL of diethyl ether, and dried in vacuo (0.1 mbar, 24 h). Yield: 249 mg (0.26 mmol, 75%). Anal. Found (calcd) for $C_{40}H_{34}N_{12}O_6S_2Fe{\cdot}2CH_3OH$ (molar mass 962.85 g mol^{-1}): C, 52.22 (52.39); H, 4.44 (4.40); N, 17.49 (17.46). FIR (in cm^{-1}): 194 (w, broad), 269 (m), 353 (w), 387 (w), 423 (m), 480 (s), 502 (m), 560 (s), 568 (s), 608 (s), 623 (m). MIR (in cm^{-1}): 674 (s), 758 (s), 790 (s), 827 (m), 884 (m), 1031 (s), 1090 (s), 1175 (s), 1234 (s), 1280 (s), 1410 (s) 1448 (m), 1624 (m), 2972 (w), 3124 (m), 3448 (m, broad). TGA: maximum decomposition rate at ∼261 °C.

Synthesis of $[Fe(NH_2trz)_3](2ns)_2$. This complex has been synthesized by a procedure modified from that described in the literature.[11] A solution containing both hexaaquairon(II) 2-naphthalenesulfonate (6.00 g, 10.4 mmol) and ascorbic acid (0.37 g, 2.1 mmol) in 300 mL of methanol was combined with a solution of 4-amino-1,2,4-triazole (2.62 g, 31.1 mmol) in 100 mL of methanol and stirred for 1 h. The white precipitate obtained was filtered off (whereupon it turned pink) and washed with 150 mL of methanol. The product was dried under vacuum (0.1 mbar, 24 h). Yield: 6.14 g (8.2 mmol, 79%). Anal. Found (calcd) for $C_{26}H_{26}N_{12}O_6S_2Fe{\cdot}1.36H_2O$ (molar mass 747.04 g mol^{-1}): C, 41.67 (41.75); H, 3.93 (3.87); N, 22.28 (22.47); O, 15.58 (15.74); H_2O, 3.27 (3.27). FIR (in cm^{-1}): 249 (w), 271 (w), 423 (m), 476 (m), 501 (w), 552 (s), 560 (s), 569 (s), 623 (s), 647 (s). MIR (in cm^{-1}): 677 (s), 747 (s), 818 (s), 863 (m), 903 (w), 1032 (s), 1137 (w), 1182 (s, broad), 1346 (m), 1504 (m), 1545 (m), 1593 (m), 1630 (m, broad), 3055−3290 (s, broad), 3468 (m, broad). TGA: loss of water at ∼77 °C (clearly H_2O is bound in the Fe^{2+}−NH_2trz complex more weakly than in liquid water); maximum decomposition rate at ∼339 °C.

Treatment of $[Fe(NH_2trz)_3](2ns)_2$ with Water. A suspension of $[Fe(NH_2trz)_3](2ns)_2$ (100 mg, 0.13 mmol) was stirred for 10 min in water (5 mL). The suspension was thereafter centrifuged for 3 min (4000 min^{-1}). The supernatant liquid was decanted, and the process was repeated. The remaining solid was suspended in 2 mL of water and stirred for 1 min. After centrifugation, the supernatant liquid was decanted, and the resulting white powder was dried in vacuo (0.1 mbar, 2 h). Yield: 9 mg (0.015 mmol). FIR and MIR spectra were identical with those described above for $[Fe(H_2O)_6](2ns)_2$. TGA: loss of water at ∼102 °C, maximum decomposition rate at ∼529 °C.

Exposure of $[Fe(NH_2trz)_3](2ns)_2$ to Ascorbic Acid. In order to investigate prevention of oxidation by ascorbic acid, solutions were prepared by mixing $[Fe(H_2O)_6](2ns)_2$ (28.6 mg, 0.049 mmol), NH_2trz (12.4 mg, 0.148 mmol, 3 equiv), and varying amounts of ascorbic acid (0 mg; 1.7 mg, 0.010 mmol, 20 mol %; 2.9 mg, 0.016 mmol, 33 mol %; 4.3 mg, 0.025 mmol, 50 mol %; 8.6 mg, 0.049 mmol, 100 mol %) in 3 mL of DMF. These solutions were stored at ambient

dx.doi.org/10.1021/ic403035u | Inorg. Chem. 2014, 53, 3546−3557

conditions in UV/vis cuvettes closed with a poly(tetrafluoroethylene) (PTFE) stopper. Photographs (taken with a Canon PowerShot S95 digital camera) and UV/vis absorption spectra were taken after 15 min, 1 h, 2 h, 4 h, 7 h, 1 d, 2 days, 4 days, 7 days, and 16 days.

In order to study the influence of water, $[Fe(H_2O)_6](2ns)_2$ (20 mg, 0.034 mmol) was dissolved in DMF (2 mL). Then 100 mg of molecular sieve (3 Å) was added and the mixture was left for 30 min. Thereafter, ascorbic acid (38 mg, 0.216 mmol, 6 equiv) was added. For comparison, the same procedure was carried out without molecular sieve.

Preparation of $[Fe(NH_2trz)_3](2ns)_2$ Films. A 48.2 mg quantity (0.0833 mmol) of $[Fe(H_2O)_6](2ns)_2$ and 21.6 mg (0.257 mmol) of NH_2trz were dissolved together in 4 mL of degassed DMF. The mixture was stirred for 20 min, resulting in a clear pink solution. This solution was cast in a Petri dish (diameter 5 cm) and subsequently exposed to a reduced pressure of ca. 1.5 mbar for 4 h, resulting in films of a thickness of ca. 60 μm.

Analysis. Infrared spectra were recorded with a Bruker Vertex 70 FTIR spectrometer. Mid-infrared (MIR) spectra were obtained in KBr with a DLaTGS detector in the range of 4000−370 cm^{-1} and far-infrared (FIR) spectra in CsI pellets with a DTGS detector in the range of 600−60 cm^{-1}. Intensities are described as follows: w, weak; m, medium; s, strong.

^{1}H NMR spectra were measured on a Bruker Ultrashield 300 MHz Fourier-transform spectrometer. The multiplicities are indicated as follows: s, singlet; d, doublet; dd, doublet of doublets.

Thermogravimetric analysis (TGA) was carried out with a TGA/SDTA851 (Mettler Toledo) instrument under a nitrogen atmosphere at a heating rate of 10 °C min^{-1}.

Elemental analyses were performed by the microanalytic laboratory of the Laboratory of Organic Chemistry (LOC), ETH Zurich.

UV/Vis Spectroscopy. Optical spectra of solutions of the various compounds were recorded with a Perkin-Elmer Lambda 900 spectrometer in a wavelength region of 475−700 nm in quartz glass cuvettes with an optical path length of 1 cm (or 2 cm for measurements with iron concentrations below 0.017 mol L^{-1}) at a scan speed of 250 nm min^{-1}, an integration time of 0.2 s, a data interval of 1 nm, a slit width of 1 nm, and a time interval of 3 min between measurements. Kinetic measurements were executed at a wavelength of 541 nm with an integration time of 5 s, a slit width of 2 nm, and a time interval of 15 s between measurements.

For kinetic measurements, a solution of hexaquairon(II) 2-naphthalenesulfonate (concentrations between 0.025 and 0.065 mol L^{-1}, volumes between 1.80 and 2.35 mL in 1 cm cuvettes and 2.35 mL in 2 cm cuvettes) and L-ascorbic acid (33 mol % with respect to Fe^{2+}; to prevent oxidation from Fe^{2+} to Fe^{3+} by molecular oxygen) in *N,N*-dimethylformamide (DMF), henceforth referred to as *solution 1*, was combined immediately before starting UV/vis measurements with a solution of 4-amino-1,2,4-triazole (concentrations between 0.101 and 0.324 mol·L^{-1}, volumes between 0.88 and 1.35 mL in 1 cm cuvettes and 1.76 mL in 2 cm cuvettes) in DMF, henceforth referred to as *solution 2*.

In the following, an example is given for a final Fe^{2+} concentration of 0.019 mol L^{-1} and a ligand to metal ratio of 3/1. *Solution 1* was prepared by dissolving $[Fe(H_2O)_6](2ns)_2$ (225.0 mg, 0.39 mmol) and L-ascorbic acid (22.5 mg, 0.13 mmol) in DMF (12 mL). To prepare *solution 2*, NH_2trz (98.1 mg, 1.17 mmol) was dissolved in DMF (9 mL). A 1.175 mL portion of *solution 1* was combined with 0.880 mL of *solution 2* (by fast addition through an Eppendorf pipet; during this process the two solutions mixed) directly before the measurement of visible absorption spectra.

Measurements with a constant ligand to metal ratio of 3/1 were performed with the following Fe^{2+} concentrations: 0.014, 0.017, 0.019, 0.021, and 0.024 mol L^{-1}.

For experiments with a constant Fe^{2+} concentration of 0.019 mol L^{-1}, the following ligand to metal ratios were employed: 1/1, 2/1, 3/1, 4/1, 5/1, 6/1, 9/1, 12/1, and 15/1.

When the Fe^{2+} solution was added in two steps, an initial reaction mixture was allowed to react for 15 min, whereupon a second portion of Fe^{2+} solution was added. These measurements were recorded with the following Fe^{2+} concentrations (mol·L^{-1}) and ligand to metal ratios: initial 0.019 (6/1), final 0.024 (3/1); initial 0.019 (9/1), final 0.024 (4.5/1); initial 0.019 (9/1), final: 0.018 (6/1).

Stepwise addition of NH_2trz was carried out analogously as described above for the stepwise addition of Fe^{2+} solutions. These experiments were performed with the following Fe^{2+} concentrations (mol·L^{-1}) and ligand to metal ratios: initial 0.037 (1.5/1), final 0.026 (3/1); and initial 0.025 (3/1), final 0.018 (6/1).

Small-Angle X-ray Scattering (SAXS). Small-angle X-ray scattering (SAXS) experiments were performed using a Rigaku MicroMax-002+ microfocused beam (40 W, 45 kV, 0.88 mA) of Cu Kα radiation ($\lambda_{Cu\ K\alpha}$ = 1.5418 Å), which was collimated by three pinhole (0.4, 0.3, and 0.8 mm) collimators. The scattered X-ray intensity was detected with a two-dimensional Triton-200 X-ray gas-filled detector (20 cm diameter, 200 μm resolution). An effective scattering vector range of 0.1 $nm^{-1} < q < 2$ nm^{-1} was obtained, where q is the scattering wave vector defined as $q = (4\pi/\lambda_{Cu\ K\alpha}) \sin\theta$, with a scattering angle of 2θ. Experiments were performed on DMF solutions of iron-based complexes at different concentrations and stoichiometric ratios between iron and ligand. Samples were placed in a self-constructed reusable capillary, and the scattering background was subtracted. Temperature was controlled by a homemade heating block connected to a F25-MC Julabo cooling/heating bath system.

X-ray Absorption Spectroscopy. X-ray absorption measurements were performed at beamline A1, Hasylab (Hamburg, Germany). A channel-cut Si(111) double-crystal monochromator was used for measurements at the Fe K-edge (7.112 keV). Measurements were carried out in transmission mode with ionization chambers filled with nitrogen. The nitrogen pressure was adjusted for optimal absorption at the Fe K-edge. Energy calibration was performed with an iron metal foil prior to the respective measurements. Solid samples were embedded in a cellulose matrix and pressed into a pellet. The embedding technique was used because measurements of neat samples are crucial due to self-absorption and particle size issues. Especially in neat samples particle size effects can lead to a significant reduction of the EXAFS amplitude and thus to severe misinterpretations (see e.g. the early work of Lu and Stern[14]). If fluorescence measurements were carried out, the problem was even enhanced, since self-absorption effects emerge that in the worst case can smear out the EXAFS signal completely. Since microcrystallinity still is present in the samples, the properties of the compound should not be affected. Note that solid samples have not been used for SCO investigations but only for comparison of data of dissolved complexes in the low-spin state: i.e., temperature-dependent measurements were not carried out. As neat powders pressed under a load of 10000 kg/cm^2 still showed the color of the low-spin state, we assume that that the pressed samples investigated with EXAFS are still in the low-spin state, all the more as the resulting Fe−Fe bond lengths were in the expected region (see below).

Samples in solution were measured in a specially designed liquid sample cell, which allowed filling under defined conditions.[15,16] Several scans were carried out and averaged for each sample, and especially for the measurements in the course of the complex formation consecutive scans were carried out to check for possible changes with time.

To determine the smooth part of the spectrum, corrected for pre-edge absorption, a piecewise polynomial was used. It was adjusted in such a way that the low-R components of the resulting Fourier transform were minimal. After division of the background-subtracted spectrum by its smooth part, the photon energy was converted to photoelectron wavenumbers k. The resulting $\chi(k)$-function was weighted with k^3.

EXAFS data analysis was performed according to the single scattering curved wave formalism of the EXCURV98 program with XALPHA phase and amplitude functions.[17] The mean free path of the scattered electrons was calculated from the imaginary part of the potential (VPI set to −4.00). The quality of fit is given in terms of the fit index $FI = \sum(\chi^{exptl} - \chi^{theor})^2 k^n / \Sigma\chi^{exp} k^n$. Since the main focus of the present work is the formation of polynuclear structures in solution, no multiple scattering analysis was carried out, since this requires the a priori knowledge of the structure investigated, which is per se

dx.doi.org/10.1021/ic403035u | Inorg. Chem. 2014, 53, 3546−3557

contradictory to a study on the formation mechanism of those structures, where unknown species may occur.[3]

Single-Crystal X-ray Structure Determination. X-ray diffraction data were collected with an Oxford Diffraction instrument equipped with an Onyx CCD detector, a molybdenum X-ray tube, and a graphite monochromator. A φ scan was performed for unit-cell determination, and the measurement strategy (ω scans) was devised by CrysAlis CCD.[18] Data reduction, as well as correction for Lorentz, polarization, and absorption effects, was performed with the software CrysAlis RED.[18] Further experimental details are given in Table 1.

Table 1. Details of the X-ray Diffraction Measurements, Data Set, and Structure Refinement

chem formula	$C_{42}H_{42}FeN_{12}O_8S_2$ (=$C_{40}H_{34}N_{12}O_6S_2Fe\cdot 2CH_3OH$)
formula wt	962.85
color/habit	pink/irregular shape
cryst dimens (mm^3)	0.30 × 0.40 × 0.60
cryst syst	triclinic
space group	$P\bar{1}$ (No. 2)
a (Å)	9.38858(5)
b (Å)	10.62813(6)
c (Å)	11.51412(6)
α (deg)	72.9455(4)
β (deg)	75.4527(4)
γ (deg)	84.9335(4)
V ($Å^3$)	1063.046(10)
Z	1
T (K)	293
λ(Mo Kα) radiation (Å)	0.71073
D_{calcd} (g cm^{-3})	1.504
μ (mm^{-1})	0.523
F(000)	500
θ_{min}, θ_{max} (deg)	4.09, 26.37
h_{min}, h_{max}; k_{min}, k_{max}; l_{min}, l_{max}	−11, +11; −14, +14; −13, +13
no. of measd rflns	88699
no. of indep rflns	4343
no. of obsd rflns ($I > 2\sigma(I)$)	4167
R_{int}, R_σ	0.0182, 0.0053
no. of params, restraints	316, 0
R1(all), R1(obsd)	0.0387, 0.0378
wR2(all), wR2(obsd)	0.1133, 0.1120
weighting scheme	$w = 1/[\sigma^2(F_o^2) + (0.0740P)^2 + 0.3006P]$ ($P = (F_o^2 + 2F_c^2)/3$)
goodness of fit GOF/S	1.085
max, av shift/error	0.001, 0.000
residual densities $\Delta\rho_{min}$, $\Delta\rho_{max}$ (e $Å^{-3}$)	−0.640, 0.463

After merging, all independent reflections were used for structure determination. The structure was solved by direct methods with the aid of successive difference Fourier analysis and refined by full-matrix least-squares refinements against F^2 using SHELXL97[19] and ShelXle.[20] All non-hydrogen atoms were refined with anisotropic displacement parameters, while hydrogen atoms were placed in calculated positions and refined using a riding model. Images were generated with CrystalMaker.[21]

Solubility Tests. An 18 mg portion of $[Fe(NH_2trz)_3](2ns)_2$ was combined with 1.6 mL of the respective solvent, and the mixture was stirred for 2 h. No significant solubility was found by visual inspection for the following solvents: acetone, acetonitrile, dichloromethane, diethyl ether, *N,N*-diethylformamide, 1,4-dioxane, methanol, tetrahydrofuran, toluene, 1,2,4-trichlorobenzene, and *p*-xylene. The last three suspensions did not lead to dissolution of the solids even after heating to 80 °C. In contrast, $[Fe(NH_2trz)_3](2ns)_2$ is slightly soluble in water and dimethyl sulfoxide (DMSO). However, it dissociates in these solvents (see text). Nonetheless, the complex is soluble in DMF, as discussed in the text.

RESULTS

Solubility of $[Fe(NH_2trz)_3](2ns)_2\cdot xH_2O$. As we are not aware of reports on the solubility of $[Fe(NH_2trz)_3](2ns)_2\cdot xH_2O$ (NH_2trz: = 4-amino-1,2,4-triazole, 2ns = 2-naphthalenesulfonate) and in fact related compounds have been found to be largely insoluble in common organic solvents,[22] we investigated this aspect first in order to enable studies in solution. It was found that $[Fe(NH_2trz)_3](2ns)_2\cdot xH_2O$ is essentially insoluble in most common organic solvents (see the Experimental Section). Slight solubility was observed in water and dimethyl sulfoxide (DMSO) at room temperature and good solubility in *N,N*-dimethylformamide (DMF) after prolonged stirring. However, while in DMF the initial pink color of the Fe^{2+}–triazole complex in the low-spin state was preserved, the water and DMSO solutions were colorless. The latter indicates either the presence of (polynuclear) structures in the high-spin state (materials which are colorless, see below) or virtually complete dissociation of $[Fe(NH_2trz)_3](2ns)_2$. We tend to assume that $[Fe(NH_2trz)_3](2ns)_2$ dissociates at least in water, as washing of $[Fe(NH_2trz)_3](2ns)_2$ with small amounts of water yielded $[Fe(H_2O)_6](2ns)_2$ (cf. the Experimental Section). Obviously, the equilibrium constants for coordination of NH_2trz to Fe^{2+} are higher in DMF than in water. Therefore, DMF was selected as the solvent for the following investigations.

As a side remark, the solubility of $[Fe(NH_2trz)_3]^{2+}$ depends strikingly on the counterion. For example, the chloride and even the 1-naphthalenesulfonate complex are virtually insoluble in DMF.

Stabilization of $[Fe(NH_2trz)_3](2ns)_2\cdot xH_2O$ Solutions in DMF with Ascorbic Acid. The stability of Fe^{2+} toward oxidation to Fe^{3+} by molecular oxygen is limited in solution, as clearly manifested by a color change from pink to brownish yellow under ambient conditions. L-Ascorbic acid has been previously used as an antioxidant during the synthesis of Fe^{2+}–triazole complexes.[11] Hereby, ascorbic acid is suggested to be oxidized in a catalytic cycle under concomitant reduction of Fe^{3+} to Fe^{2+}.[23]

Oxidation under ambient conditions can be readily monitored by UV/vis spectroscopy, since $[Fe(NH_2trz)_3](2ns)_2$ dissolved in DMF shows a pronounced absorption maximum at 541 nm, while oxidation to Fe^{3+} species leads to increase in absorption between 400 and 500 nm, however, without a pronounced maximum at higher levels of oxidation (broad absorption band, see Figure SI-1 in the Supporting Information). Thus, solutions of Fe^{2+} with 3 equiv of NH_2trz in DMF, without and with ascorbic acid (33% mol/mol with respect to Fe^{2+}) were freshly prepared, poured into quartz glass cuvettes, and analyzed with UV/vis spectroscopy between 15 min and 5 days after sample preparation. While the solutions were still pink in the presence of ascorbic acid after 4 days, they turned brown already after 7 h in the absence of ascorbic acid. These color changes and corresponding UV/vis spectra imply that solutions with 20% mol/mol ascorbic acid already show distinct oxidation of Fe^{2+} after 1 day, while this oxidation appeared at 50% mol/mol only after 7 days, and at 100% mol/mol the pink appearance was still preserved after 16 days.

It is of note that ascorbic acid is, under certain conditions, able to coordinate to Fe^{2+} (indeed only in the presence of molecular oxygen), which is associated with a purple color in

dx.doi.org/10.1021/ic403035u | Inorg. Chem. 2014, 53, 3546−3557

aqueous solution.[24] Hence, experiments were carried out to investigate coordination of ascorbic acid in DMF, using the same iron source and similar concentrations (0.0185 mol L^{-1} of Fe^{2+}) (also used for the following studies). Addition of ascorbic acid to solutions of $[Fe(H_2O)_6](2ns)_2$ in DMF did not lead to a color change, even with a large excess of ascorbic acid (6 equiv with respect to Fe^{2+}). However, remarkably, if water molecules originating from $[Fe(H_2O)_6](2ns)_2$ were removed by addition of molecular sieve (3 Å), the solution turned purple (cf. broad absorption band in UV/vis spectra with a maximum at 530 nm; see Figure SI-3 in the Supporting Information) already in the presence of 3 equiv of ascorbic acid. Thus, it appears that a small amount of water prevents coordination of ascorbic acid to Fe^{2+} under the conditions applied here.

Formation of Iron(II) 4-Amino-1,2,4-triazole Complexes in DMF: Dependence on Concentration. Visible absorption spectroscopy was employed to monitor the formation of Fe^{2+}–NH_2trz complexes by a combination of $[Fe(H_2O)_6](2ns)_2$ and NH_2trz, as the last two compounds do not notably absorb in the UV/vis spectral regime, while a peak at 541 nm developed upon combination (Figure 2).

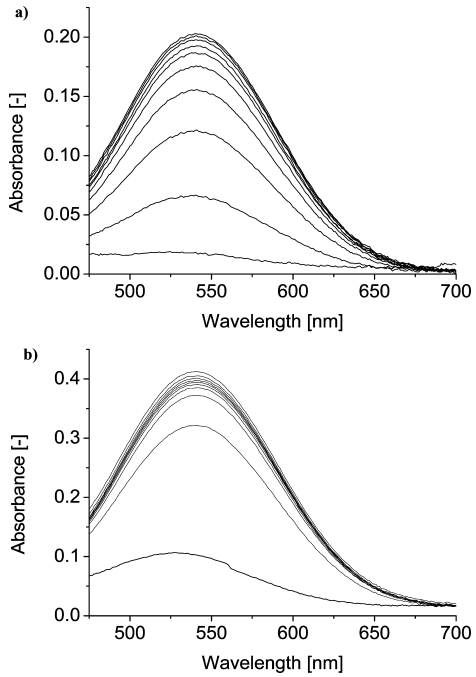

Figure 2. Visible absorption spectra recorded during the reaction of $[Fe(H_2O)_6](2ns)_2$ and NH_2trz (NH_2trz/Fe^{2+} 3/1) in DMF at time intervals of 3 min and a recording time for each measurement of 54 s. The first measurement started 20 s after mixing the solutions; the total reaction time was 30 min. Fe^{2+} concentrations: (a) 0.0165 mol L^{-1}, (b) 0.0236 mol L^{-1}.

Accordingly, investigations were performed at concentrations suited for detection with UV/vis spectroscopy: i.e., at Fe^{2+} concentrations on the order of 0.02 mol L^{-1}. When spectra were recorded for 30 min at time intervals of 3 min, formation of Fe^{2+}–NH_2trz complexes continuously proceeded during the scan period (each scan took 54 s). However, in particular at high concentrations, reactions were fast with respect to spectral recording. As a consequence, the peak maximum in the first spectrum (start of recording 20 s after start of the reaction) appears to be shifted toward lower wavelengths. Naturally, a kink arose at 561 nm in the spectrum due to a short interruption of the measurement (inherent in the spectrometer), during which the reaction proceeded. At high concentrations the complexes tended to slowly form gels, which resulted in pronounced scattering of light, manifested in an increase in absorbance over the whole spectral range. Evidently, the above issues render interpretation of related spectra somewhat delicate.

To investigate the actual formation of linear compounds (polymers), first the concentration of Fe^{2+} was changed in a relatively narrow range at a constant molar NH_2trz/Fe^{2+} ratio of 3/1. Spectra were recorded during the reaction of Fe^{2+} and NH_2trz at four different concentrations of Fe^{2+}: i.e. c_{Fe} = 0.0165, 0.0185, 0.0206, 0.0236 mol·L^{-1}. The absorbance increased with increasing reaction time and iron concentration, while importantly, the absorption maximum wavelength (λ_{max}) did not change significantly. Two series of spectra as a function of time representing the highest and lowest Fe^{2+} concentrations, respectively, are shown in Figure 2. The increase in absorption effectively saturated after 20 min at c_{Fe} = 0.0165 mol L^{-1} and after 10 min at c_{Fe} = 0.0236 mol L^{-1}, respectively: i.e., the rate of plateau formation of the absorbance increased with increasing Fe^{2+} concentration. Hence, the UV/vis spectra provide evidence for the formation of low-spin Fe^{2+}–NH_2trz complexes in DMF (high-spin complexes are essentially colorless; see below).

Structure Analysis. In order to obtain information about the structure and shape of the above complexes in solution, small-angle X-ray scattering (SAXS) experiments were performed on solutions of three different concentrations (c_{Fe} = 0.0165, 0.0185, and 0.0206 mol L^{-1}, molar NH_2trz/Fe^{2+} ratio of 3/1). Figure 3 shows a double-logarithmic plot of the radial

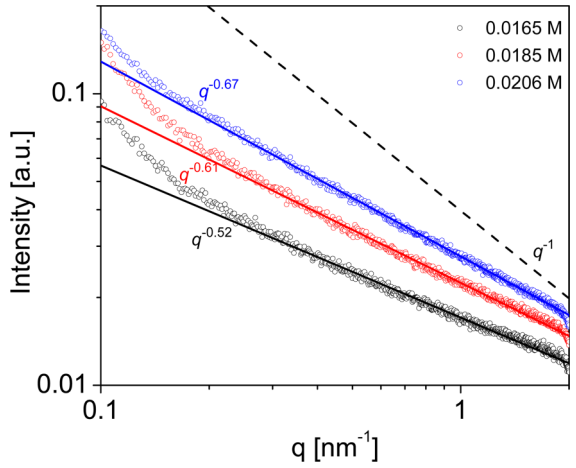

Figure 3. 1D radial scattering intensity distribution for three different iron concentrations at a 3/1 molar ratio of NH_2trz/Fe.

scattering intensity distribution of the solutions. The absolute value of the slope of the individual curves (in the range 0.3 nm^{-1} < q < 1.5 nm^{-1}) increased with increasing Fe^{2+} concentration; yet the slopes differed from the characteristic value of rigid rods (−1). As will be supported below in the form of experiments, the absolute value of the slope of a value below −1 indicates the coexistence of long stiff objects (polymers) and shorter species (oligomers) whose contour length is well below the persistence length of the polynuclear objects. The overall scattering profile in this q region then results from the sum of the −1 slope of larger linear entities and that associated

dx.doi.org/10.1021/ic403035u | Inorg. Chem. 2014, 53, 3546−3557

with the envelope merging the individual Guinier regimes of the smaller sequences. Thus, the resulting average slope differing from −1 is simply the signature of the equilibrium nature of the coordination compounds studied here. Nonetheless, the results imply that an increase in concentration favors the formation of linear stiff entities (still at NH_2trz/Fe^{2+} 3/1): i.e., more concentrated samples induce a shift of the equilibrium toward larger populations of longer objects, resulting in increased slopes in absolute values.

NH_2trz/Fe^{2+} Ratio. Variation of the ligand to metal ratio was implemented at an Fe^{2+} concentration of 0.0185 mol L^{-1} by changing the amount of NH_2trz: i.e., NH_2trz/Fe^{2+} ratios from 1/1 to 15/1 (a ratio of 3/1 corresponds to the ratio in a polynuclear Fe^{2+} triazole complex in the solid state). In addition to acquisition of UV/vis absorption spectra, absorbance measurements at a single wavelength (λ_{max}) were also collected at time intervals of 15 s in order to follow the kinetics of complex formation more accurately (Figure 4). At a ratio of 1/1

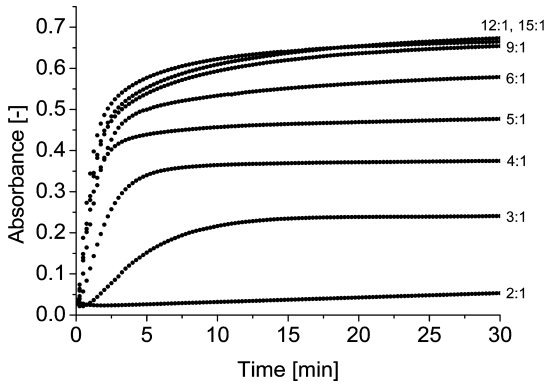

Figure 4. Absorbance at 541 nm during the reaction of $[Fe(H_2O)_6](2ns)_2$ and NH_2trz in DMF (resulting Fe^{2+} concentration: 0.0185 mol L^{-1}) at molar NH_2trz/Fe^{2+} ratios of 2/1, 3/1, 4/1, 5/1, 6/1, 9/1, 12/1 and 15/1, measured at time intervals of 15 s and an integration time of 5 s. The first measurement started 20 s after mixing the solutions; the total reaction time was 30 min. The measurement with 1 equiv of NH_2trz is not shown, as it essentially coincides with the baseline.

no significant absorption was detected in the investigated spectral range of 475−700 nm. At a ratio of 2/1 a minor peak appeared at 541 nm; the intensity of this peak at the end of the observed time interval of 30 min increased with increasing ligand to metal ratio up to around 10 equiv of NH_2trz and then remained nearly constant at higher ratios. This peak developed more quickly at higher NH_2trz/Fe^{2+} ratios. Accordingly, at a ratio of 2/1, the plateau value was very low and was not reached within 30 min. At NH_2trz/Fe^{2+} ratios of 6/1 and above, the absorbance increased slightly beyond the time expected to attain the plateau value, on the basis of the rates observed for NH_2trz/Fe^{2+} ratios from 2/1 to 5/1. Hence, a relatively slow process seems to interfere with complex formation, which might be associated with the formation of aggregates (see the Supporting Information).

Samples prepared with different NH_2trz/Fe^{2+} ratios, ranging from 3/1 to 9/1, were studied also by means of SAXS (c_{Fe} = 0.0185 M). The same slope analysis as described above was performed for this set of compounds; the slope's absolute values and the intensities at low q values increased upon increasing the NH_2trz/Fe^{2+} ratio (Figure 5). At a ratio of 9/1, the evaluated slope from the SAXS intensity profile amounted almost to −1, confirming the shift of the equilibrium toward

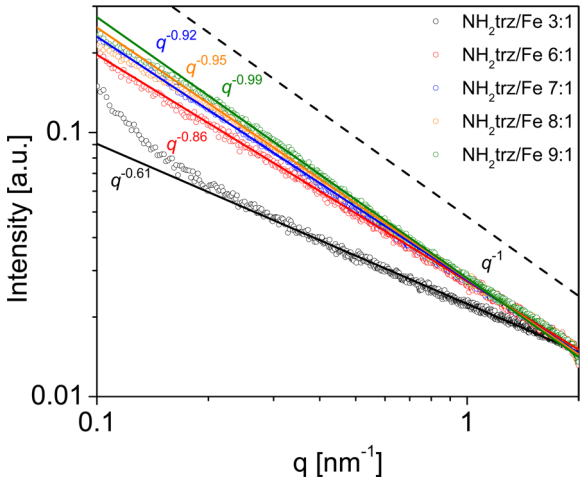

Figure 5. 1D radial scattering intensity distribution for molar NH_2trz/Fe^{2+} ratios of 3/1, 6/1, 7/1, 8/1 and 9/1, at a total iron(II) concentration of 0.0185 mol L^{-1}.

linear stiff objects upon increase of the NH_2trz/Fe^{2+} ratio. Those rods are estimated to have a minimum length of 30 nm and an aspect ratio of approximately 50 minimum (Figure SI-4, Supporting Information), which roughly corresponds to a minimum of 100 iron(II) atoms per polynuclear object.

Spin State. Insight into the spin state of polymeric Fe^{2+} complexes with NH_2trz in the solid state was reported on the basis of XANES (X-ray absorption near edge structure) and EXAFS (extended X-ray absorption fine structure) spectroscopy.[3,27] Accordingly, we used these techniques to gain information about the spin state of related metal centers in solution. High-spin and low-spin Fe^{2+} complexes in an octahedral environment can be distinguished in the XANES spectra by means of the pre-edge signal (prepeak) and the white line shape: i.e., the first resonances after the edge jump.[3,25] For an octahedral $3d^6$ system the lower-lying t_{2g} orbitals are partially empty in the high-spin state (in contrast to the low-spin state) and thus available for excitations only in the high-spin state; therefore, excitations at lower energy are expected for the high-spin spectrum in comparison to that of the low-spin state. Multiplet calculations for $1s^23d^6 \rightarrow 1s^13d^7$ transitions in an octahedral crystal field reveal the underlying excitations that determine the spectra. These are transitions from the $^5T_{2g}$ quintet ground state to the $^4T_{1g}$, $^4T_{2g}$, and $^4T_{1g}$ quartet states for the high-spin form and from the $^1A_{1g}$ to the ^2E_g doublet state for the low-spin form.[25] The structure of the high-spin spectrum is not resolved in XANES spectra, because of the short lifetime of the 1s core hole leading to a natural line width of 1.3 eV.[26]

In Figure 6, the XANES spectra of solutions containing different NH_2trz/Fe^{2+} ratios are compared with the spectrum of the Fe^{2+} precursor, $[Fe(H_2O)_6](2ns)_2$, in the solid state and in DMF solution (c_{Fe} = 0.0185 mol L^{-1}). It is obvious that dissolution of $[Fe(H_2O)_6](2ns)_2$ led to reduced white line intensity and a slightly shifted edge to lower energies. Adding the first equivalent ligand did not affect the spectrum. All spectra mentioned so far were of high-spin character, as was evident from the single broad prepeak[25] in the enlarged prepeak area and the characteristic white line shape.[27] Adding the third equivalent of ligand induced significant changes in the white line, which was reduced in intensity and split into two signals. These phenomena can be explained by a mixture of

dx.doi.org/10.1021/ic403035u | Inorg. Chem. 2014, 53, 3546−3557

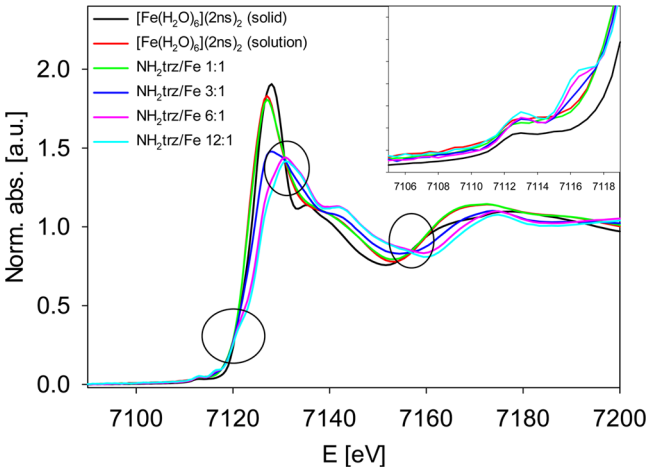

Figure 6. XANES spectra recorded after addition of 1, 3, 6, and 12 equiv of NH_2trz to a solution of $[Fe(H_2O)_6](2ns)_2$. For comparison the spectra of $[Fe(H_2O)_6](2ns)_2$ in the solid and dissolved states are also shown. Isosbestic points are highlighted, and the prepeak area is shown enlarged in the inset.

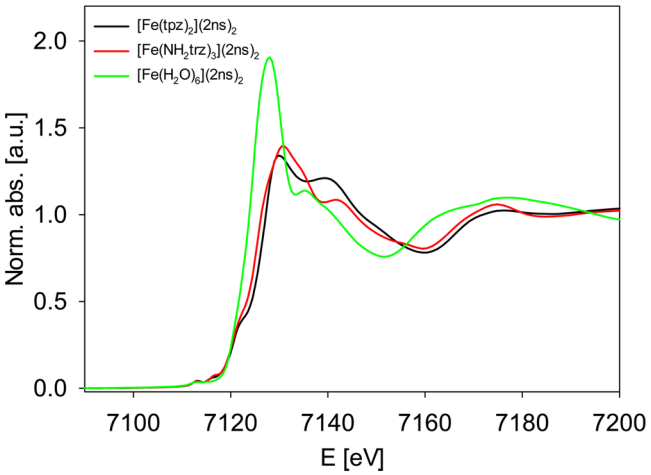

Figure 7. XANES spectra of the solid products $[Fe(tpz)_2](2ns)_2$ (mononuclear) and $[Fe(NH_2trz)_2](2ns)_2$ (polynuclear). The spectrum of $[Fe(H_2O)_6](2ns)_2$ is also shown for comparison.

high-spin and low-spin states. Fitting the spectrum using a linear combination approach[28] with $[Fe(H_2O)_6](2ns)_2$ and a solution with NH_2trz/Fe^{2+} ratio of 12/1 as references for pure high-spin and low-spin states, respectively, reveals a high-spin/low-spin ratio of 0.45/0.55 at a NH_2trz/Fe^{2+} ratio of 3/1. Moreover, the prepeak at around 7113 eV sharpens and a shoulder at around 7116.5 eV appears. These two facts indicate in the average a transition state between high-spin and low-spin states (the structure will be analyzed closer in the EXAFS section). At NH_2trz/Fe^{2+} ratios of 6/1 and 12/1 the iron centers are essentially present in the low-spin state; no significant differences between these two ratios were observed, apart from a slight difference in white line intensity and peak width of the two prepeaks. Notably, the presented set of solution state spectra exhibits isosbestic points, which indicate that the Fe^{2+}/NH_2trz system is in an equilibrium and that no removal of X-ray absorption centers from the solution (i.e., by precipitation) occurred.[16]

For comparison, the mononuclear complex $[Fe(tpz)_2](2ns)_2$ (where tpz = tris(pyrazolyl)methane) was synthesized and its structure was determined by single-crystal X-ray diffraction. A slightly distorted octahedral coordination was found with three different Fe−N distances between 1.97 and 1.98 Å (Table SI-1, Supporting Information). Structural data are shown in Table 1, and a schematic of the structure is shown in Figure SI-2 (Supporting Information). In comparison to the polynuclear complex $[Fe(NH_2trz)_3](2ns)_2$, $[Fe(tpz)_2](2ns)_2$ showed an increased solubility in organic solvents. In addition to DMF, it was found to be soluble in dichloromethane and methanol, while it turned out to be insoluble in acetone, water, diethyl ether, and toluene. $[Fe(tpz)](2ns)_2$ was thermally stable up to 200 °C and did not show any color change up to this temperature, in contrast to the case for $[Fe(NH_2trz)_3](2ns)_2$. In Figure 7, XANES spectra of the solid samples of this complex and $[Fe(NH_2trz)_3](2ns)_2$ as well as of $[Fe(H_2O)_6](2ns)_2$ are compared. It is obvious that both $[Fe(tpz)_2](2ns)_2$ and $[Fe(NH_2trz)_3](2ns)_2$ are low-spin compounds, due to the characteristic shape and prepeak splitting in XANES spectra. However, differences between the mononuclear $[Fe(tpz)_2](2ns)_2$ and the polynuclear $[Fe(NH_2trz)_3](2ns)_2$ exist in the intensity ratio of the XANES signals at around 7130 and 7140 eV, as well as in the intensity of the prepeak at 7116.5 eV. Since these signals are caused by multiple scattering, the differences are explained by a different polynuclearity degree of the iron scaffold. It will be shown in the EXAFS analysis (see below) that these differences are mainly due to the mononuclear and polynuclear iron scaffold.

Table 2 summarizes the structural parameters obtained by fitting the experimental EXAFS spectra with theoretical models. The corresponding spectra are presented in Figure SI-5 (Supporting Information). $[Fe(H_2O)_6](2ns)_2$ in the solid state could only be fitted with a single oxygen shell comprising six neighboring atoms. This situation changes in DMF solution, where an additional Fe−C contribution is detected, indicating that DMF molecules coordinate to the iron center. Addition of the first equivalent of NH_2trz to Fe^{2+} did not induce any significant change in the EXAFS spectra. This situation was drastically altered in presence of 3 equiv of NH_2trz. Now, a five-shell model is required to approximate the experimental spectra. The nearest-neighbor contribution is split into two Fe−N shells around 2.0 and 2.2 Å, in agreement with the distance for low-spin and high-spin complexes of that type.[3]

The corresponding coordination numbers of 2.5 and 3.3 reflect very well the high-spin/low-spin ratio of 0.45/0.55, which was obtained by quantification of the XANES spectra. With higher uncertainty, this can also be stated about the higher Fe−Fe shells, the distances of which (3.3 and 3.9 Å) are also in agreement with high-spin and low-spin distances.[3] It can thus be concluded that at the ratio of NH_2trz/Fe^{2+} = 3/1 high-spin and low-spin structures are formed and that NH_2trz is the dominant ligand, which is obvious from the light-atom shell at 3.1 Å. Since C and N cannot be distinguished by EXAFS, this shell is assigned to a combined Fe−C+N contribution of the aminotriazole ligand. Further, an individual Fe^{2+} ion is bound in the average approximately to one Fe^{2+} ion in the high-spin and one in the low-spin state: i.e., the Fe^{2+} ions are predominantly part of polynuclear structures. This follows also from a comparison with results published by Yokoyama et al., where signals in the Fourier transformed EXAFS spectra at $R > 4$ Å are explained by polynuclear structures.[3] In contrast, a multiple scattering signal at 7 Å as proposed by Michalowicz[4] could not be observed throughout the whole study and accordingly could not be fitted. We attribute this to a rather large thermal motion,

dx.doi.org/10.1021/ic403035u | Inorg. Chem. 2014, 53, 3546−3557

Table 2. Structural Parameters Obtained by Fitting the Experimental EXAFS Functions with Theoretical Models (See Text)

sample	Abs−Bs[a]	N(Abs)[b]	R(Abs-Bs)[c]/Å	σ^d/Å^{-1}	E_f^e/eV, R^f/%
$[Fe(H_2O)_6](2ns)_2$ (**1**)	Fe−O	6.1 ± 0.6	2.11 ± 0.02	0.087 ± 0.009	6.0, 20.5
$[Fe(H_2O)_6](2ns)_2$ in DMF (0.0185 mol L^{-1}) (**2**)	Fe−O	6.2 ± 0.6	2.11 ± 0.02	0.100 ± 0.010	4.1, 30.7
	Fe−C	6.2 ± 0.6	3.02 ± 0.03	0.112 ± 0.011	
$[Fe(H_2O)_6](2ns)_2$ in DMF (0.0185 mol L^{-1}), NH_2trz/Fe^{2+} = 1/1 (**3**)	Fe−O	6.1 ± 0.6	2.11 ± 0.02	0.100 ± 0.010	4.1, 32.6
	Fe−C	6.1 ± 0.3	3.02 ± 0.03	0.071 ± 0.007	
$[Fe(H_2O)_6](2ns)_2$ in DMF (0.0185 mol L^{-1}), NH_2trz/Fe^{2+} = 3/1 (**4**)	Fe−N	3.3 ± 0.3	2.03 ± 0.02	0.084 ± 0.008	3.8, 31.3
	Fe−N	2.5 ± 0.3	2.20 ± 0.02	0.084 ± 0.008	
	Fe−C + Fe−N	11.0 ± 1.1	3.06 ± 0.03	0.112 ± 0.011	
	Fe−Fe	1.3 ± 0.2	3.31 ± 0.03	0.089 ± 0.018	
	Fe−Fe	1.3 ± 0.2	3.94 ± 0.04	0.112 ± 0.022	
$[Fe(H_2O)_6](2ns)_2$ in DMF (0.0185 mol L^{-1}), NH_2trz/Fe^{2+} = 6/1 (**5**)	Fe−N	6.0 ± 0.6	1.98 ± 0.02	0.074 ± 0.007	6.6, 26.5
	Fe−C + Fe−N	12.1 ± 1.2	3.00 ± 0.03	0.097 ± 0.010	
	Fe−Fe	1.8 ± 0.2	3.32 ± 0.03	0.105 ± 0.021	
$[Fe(H_2O)_6](2ns)_2$ in DMF (0.0185 mol L^{-1}), NH_2trz/Fe^{2+} = 12/1 (**6**)	Fe−N	6.0 ± 0.6	1.97 ± 0.02	0.067 ± 0.007	6.5, 28.9
	Fe−C + Fe−N	12.0 ± 1.2	3.00 ± 0.03	0.092 ± 0.010	
	Fe−Fe	2.2 ± 0.2	3.33 ± 0.03	0.112 ± 0.022	
$[Fe(tpz)_2](2ns)_2$ (**7**)	Fe−N	6.0 ± 0.6	1.96 ± 0.02	0.045 ± 0.005	6.8, 24.4
	Fe−C + Fe−N	11.6 ± 1.2	2.91 ± 0.03	0.100 ± 0.010	
$[Fe(NH_2trz)_3](2ns)_2$ (**8**)	Fe−N	6.0 ± 0.6	1.99 ± 0.02	0.077 ± 0.008	6.0, 32.2
	Fe−C + Fe−N	12.0 ± 1.2	3.02 ± 0.03	0.087 ± 0.009	
	Fe−Fe	2.5 ± 0.3	3.29 ± 0.03	0.112 ± 0.022	

[a]Abs = X-ray absorbing atom, Bs = backscattering atom (neighbor). [b]Number of neighboring atoms. [c]Distance between Abs and Bs. [d]Debye−Waller-like factor to account for disorder. [e]Shift between experimental and calculated spectra. [f]Quality of fit.

which is reflected in the high Debye−Waller-like factor of the Fe−Fe contribution. However, it is not possible to decide if a mixture of pure high-spin and pure low-spin complexes is present or if both high-spin and low-spin states occur in the same polynuclear chain. With 6 and 12 equiv of NH_2trz, only low-spin structure parameters were obtained, in accordance with the XANES analysis. The structural number of the last two Fe−C contributions in this case is not reliable, since low-Z backscatterers exhibit a large error at such distances.[29] However, these shells are in agreement with results from single-crystal X-ray diffraction of the mononuclear complex $[Fe(tpz)_2](2ns)_2$, considering that the error margin for the number of C atoms in this shell is relatively high and that the distances are average values. The mononuclear character of $[Fe(tpz)_2](2ns)_2$ is also proven by the EXAFS results, where no Fe−Fe contribution could be detected. The structural parameters in the samples with NH_2trz/Fe^{2+} = 6/1 and 12/1 are also evident in solid $[Fe(NH_2trz)_3](2ns)_2$, but in this sample the Fe−C shell is better established due to a confined thermal motion in comparison to the solution samples.

Reversibility of Iron(II)−NH_2trz Complex Formation. First, the reversibility of complex formation was examined by dilution of Fe^{2+}−NH_2trz complexes at an NH_2trz/Fe^{2+} ratio of 3/1. For this purpose, a solution of NH_2trz and Fe^{2+} was allowed to react for 15 min (0.0185 mol L^{-1} Fe^{2+}). During this period, Fe^{2+}−NH_2trz compounds formed and accordingly the absorption band in UV/vis spectra evolved as described above, as reflected by the temporal course of absorbance at λ_{max} in Figure 8. Thereafter, DMF was added to generate a final Fe^{2+} concentration of 0.0130 mol L^{-1}. Upon dilution, the absorbance decreased during 15 min to a value of around 0.04 (Figure 8a). This value was close to the plateau value and was in agreement with the value obtained when 3 equiv of NH_2trz was exposed to a 0.0130 mol L^{-1} Fe^{2+} solution for 30 min. Note that the sharp decrease in absorbance immediately after solvent addition is caused by dilution. This is evident from

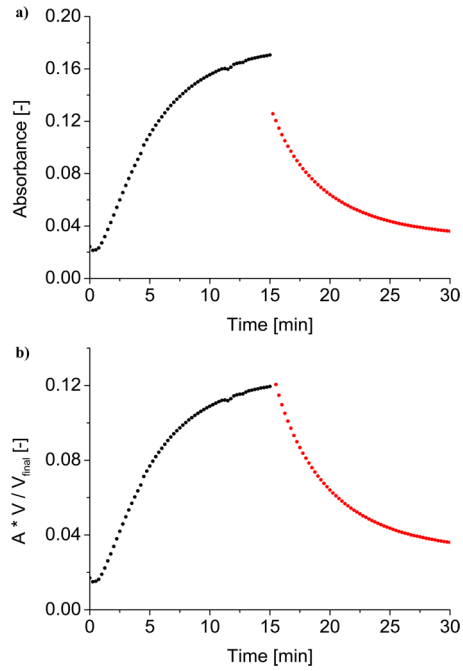

Figure 8. Absorbance at 541 nm (λ_{max}) recorded during the reaction of $[Fe(H_2O)_6](2ns)_2$ and NH_2trz in DMF, with NH_2trz/Fe^{2+} = 3/1 and Fe^{2+} concentration 0.019 mol L^{-1}. Dilution with DMF by a factor of 1.4 after 15 min: (a) absorbance; (b) normalized absorbance, taking into account the change in volume (at 15 min) upon dilution.

Figure 8b, which represents absorbance values of the initial solution calculated for the final volume after dilution: i.e., the dilution effect was compensated by multiplying the absorbance by the ratio of the respective volume and the final volume, V/V_{final}. This figure shows that complex formation, in fact, proceeded gradually.

dx.doi.org/10.1021/ic403035u | Inorg. Chem. 2014, 53, 3546−3557

Further, either Fe^{2+} solution or NH_2trz solution was added in two steps. Thus, a mixture with a ligand to metal ratio of 9/1 (c_{Fe} = 0.0185 mol L^{-1}) was first allowed to react for 15 min. Thereafter, another 0.5 equiv of Fe^{2+} (c_{Fe} = 0.0162 mol L^{-1}) was added, which led to a final Fe^{2+} concentration of 0.0176 mol L^{-1} and a ligand to metal ratio of 6/1. As a countermove, experiments were started with a ligand to metal ratio of 3/1 (Fe^{2+} concentration 0.0253 mol L^{-1}), and after 15 min 3 equiv of NH_2trz was added, which resulted, as in the above experiment, in a final Fe^{2+} concentration of 0.0176 mol L^{-1} and a ligand to metal ratio of 6/1. While the first step of each of the two experiments displayed a different development of the absorbance at λ_{max} (Figure 9), due to the different

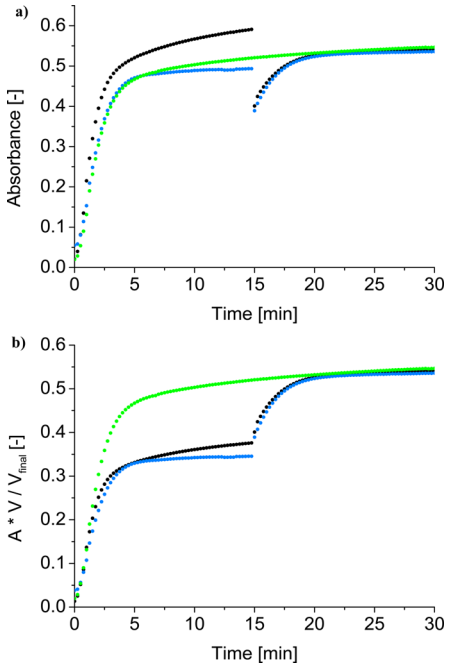

Figure 9. Absorbance at 541 nm (λ_{max}) during reactions of $[Fe(H_2O)_6](2ns)_2$ and NH_2trz in DMF: (a) absorbance values as recorded; (b) normalized absorbance, taking into account the change in volume upon dilution at 15 min. Black dots denote 0.019 mol L^{-1} Fe^{2+}, NH_2trz/Fe^{2+} = 9/1. Addition of another 0.5 equiv of dissolved Fe^{2+} after 15 min, resulting final Fe^{2+} concentration: 0.018 mol L^{-1}, NH_2trz/Fe^{2+} = 6/1. Blue: Fe^{2+} 0.025 mol L^{-1}, NH_2trz/Fe^{2+} = 3/1. Addition of 3 mol equiv of dissolved NH_2trz after 15 min. Resulting final Fe^{2+} concentration: 0.018 mol L^{-1}, NH_2trz/Fe^{2+} = 6/1. Green: Fe^{2+} 0.018 mol L^{-1}, NH_2trz/Fe^{2+} = 6/1.

concentrations, the course of the absorbance during the second step of each experiment coincided irrespective of the preceding concentrations and ligand to metal ratios. For comparison, a one-step experiment was carried out starting with the same Fe^{2+} concentration (0.0176 mol L^{-1}) and ligand to metal ratio of 6/1 as were present after the second step in both of the above sequential experiments. After a total reaction time of ca. 20 min, the same plateau value of the absorbance arose in all three cases, and the three UV/vis spectra (Figure SI-6, Supporting Information) were virtually identical. When the absorbances in the first step of the sequential reactions were converted to values considering dilution (cf. above), the absorbances in both two-step experiments increased after the first step (Figure 9b). This discloses that the intensities of the color centers increased during the second step in both two-step experiments until they reached the value of the related one-step experiment, as expected for equilibrium reactions.

As equilibria are expected to depend on temperature, a sample with an Fe^{2+} concentration of 0.0185 mol L^{-1} and a stoichiometric ratio of NH_2trz/Fe^{2+} of 9/1 was studied with SAXS at room temperature, at 60 °C, and after cooling again to room temperature. This temperature increase resulted in a discoloration of the solution, due to the transition of the colored low-spin state to the rather colorless high-spin state.[6,30] The solution was almost colorless already at temperatures above 50 °C, which indicates that high-spin states dominated. SAXS experiments revealed that an increase in temperature above this thermochromic transition shifts the equilibrium toward shorter objects, as observed from the value of the slope in a double-logarithmic plot of the scattering intensity vs q of −0.56 (Figure 10), and upon cooling the sample back to room

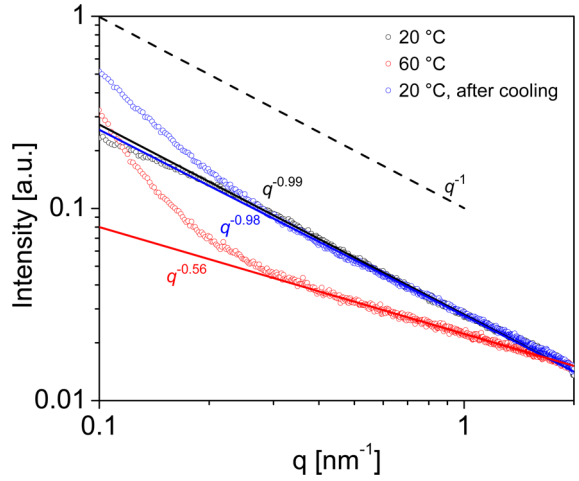

Figure 10. 1D radial scattering intensity distribution at different temperatures of $[Fe(NH_2trz)_2](2ns)_2$ at a total Fe^{2+} concentration of 0.0185 M and NH_2trz/Fe^{2+} = 9/1.

temperature an initial value of −0.99 was recovered. In addition to the analysis of the slope, at low $-q$ values, an increase in the scattering intensity was also noticed and attributed to the presence of aggregates, as shown in the case where low Fe^{2+} concentration (Figure SI-7, Supporting Information), low NH_2trz/Fe^{2+} ratio value (Figure SI-8, Supporting Information), or insufficient time for the recovery of the initial linear polymeric structure (Figure SI-9, Supporting Information) led to the presence of nonlinear structures. Thus, at higher temperatures, where the polynuclear Fe^{2+} triazole complex is in its high-spin state, the stiff linear assemblies appear to dissociate reversibly into smaller entities, which then undergo aggregation at larger length scales (i.e., at lower scattering vectors).

Films. As a side effect of this study, DMF solutions of polynuclear Fe^{2+} triazole complexes were used for the preparation of $[Fe(NH_2trz)_3](2ns)_2$ films. When such solutions were cast in Petri dishes followed by removal of solvent under reduced pressure at ambient temperature, films with thicknesses on the order of 60 μm were obtained. Notably, the color change characteristic for spin crossover in powders of $[Fe(NH_2trz)_3](2ns)_2$ upon heating to 60 °C also emerged in the films (Figure 11).

dx.doi.org/10.1021/ic403035u | Inorg. Chem. 2014, 53, 3546−3557

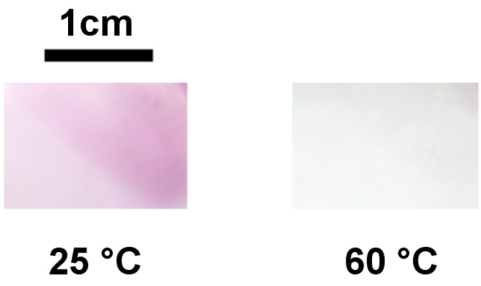

Figure 11. Optical image of a film (thickness about 60 μm) prepared from DMF solution (concentration 0.0208 M) at an NH_2trz/Fe^{2+} ratio of 3/1 and at temperatures of 25 and 60 °C, respectively.

DISCUSSION

The above results demonstrate that polynuclear coordination compounds of the type $[Fe(NH_2trz)_3]^{2+}$ can exist in solution, by the example of DMF as the solvent and Fe^{2+} concentration ranges suited for investigations with UV/vis spectroscopy (i.e. around 0.02 M). The polynuclear complexes form upon addition of NH_2trz to $[Fe(H_2O)_6](2ns)_2$ solution. However, the latter species dissolves in DMF under ligand exchange, yielding $[Fe(DMF)_6]^{2+}$. Basically, DMF can coordinate via the nitrogen or oxygen atom. In the former case EXAFS would provide 18 carbon atoms in the second coordination sphere while 6 carbon atoms should emerge in the latter case. Since 6 carbon atoms were found, we conclude that coordination of DMF proceeds via oxygen atoms, as usual in crystals containing $[Fe(DMF)_6]^{2+}$ units.[31−38] The Fe−O bond length of 2.11 Å extracted from EXAFS for $[Fe(DMF)_6]^{2+}$ in DMF solution is in the range of corresponding values found in crystals of $[Fe(DMF)_6]^{2+}$ salts (2.06−2.15 Å).[31−38] Moreover, XANES spectra reveal that the complex $[Fe(DMF)_6]^{2+}$ in DMF solution is in the high-spin state and accordingly absorbance in UV/vis spectra is negligible in the investigated spectral range.

Upon addition of 1 molar equiv of NH_2trz to $[Fe(DMF)_6]^{2+}$, DMF still dominates the coordination sphere, as indicated by EXAFS spectroscopy. A ligand/metal ratio of 3/1 corresponds to the stoichiometry of the solid $[Fe(NH_2trz)_3](2ns)_2$ coordination compound. We used UV/vis spectroscopy, XANES spectroscopy, and SAXS patterns to investigate related solutions. Accordingly, NH_2trz has indeed become the dominant ligand at the Fe^{2+} centers at an NH_2trz/Fe^{2+} ratio of 3/1 in solution, yet polymers and oligomers coexist in those conditions, and the final Fe−Fe distances of around 3.32 Å and Fe−N distances of around 1.97 Å have not yet been fully established.

When equilibrated solutions with a ligand/metal ratio of 3/1 are diluted, the fraction of polymers with Fe^{2+} ions in the low-spin state decreases to the quantity obtained in the case of direct preparation from the corresponding amounts of the Fe^{2+} salt and NH_2trz. Further, addition of Fe^{2+} to an equilibrated NH_2trz/Fe^{2+} 9/1 solution to yield a final NH_2trz/Fe^{2+} ratio of 6/1 led to the same result as corresponding addition of NH_2trz to an equilibrated NH_2trz/Fe^{2+} 3/1 solution or direct preparation of a NH_2trz/Fe^{2+} 6/1 solution from Fe^{2+} and NH_2trz. Thus, in all those cases the state of the final solutions is independent of the method of preparation or of the state of previous equilibria. These findings are in agreement with reversible processes leading to the same equilibria at the same final Fe^{2+}/NH_2trz ratio and concentration. Reversibility is also evident when the temperature of solutions is varied. An increase in temperature leads to a decrease in the object length and subsequent cooling again to an increase in length.

However, the increase in absorbance in UV/vis spectra was not compatible with first-order or second-order kinetics. This observation suggests that complex formation is not determined by a single rate-determining step. In fact there are numerous potential reactions with corresponding equilibrium constants. Some equilibria which involve coordination of NH_2trz to polynuclear iron(II) complexes might be favored for entropic reasons, analogous to the chelating effect, as illustrated by the example:

$$[Fe_2(DMF)_{10}(\mu\text{-}NH_2trz)]^{4+} + NH_2trz \rightarrow [Fe_2(DMF)_8(\mu\text{-}NH_2trz)_2]^{4+} + 2DMF$$

As two DMF molecules are mobilized upon coordination of one NH_2trz molecule, the number of species increases in the above reaction, which should favor product formation due to a gain in entropy. At an NH_2trz/Fe^{2+} ratio of 3/1, SAXS measurements imply that the equilibrium situation includes the coexistence of rigid-rod structures and smaller species.

It is expected that higher concentrations (at constant NH_2trz/Fe^{2+} ratios) or higher NH_2trz/Fe^{2+} ratios (at constant Fe^{2+} concentrations) shift the equilibrium toward polynuclear structures which come closer to the ideal linear structure. Indeed, as is evident from UV/vis spectra and SAXS analysis, at NH_2trz/Fe^{2+} = 6/1 the equilibrium is shifted considerably toward the polynuclear rigid-rod entities. Within the experimental precision of EXAFS, the coordination sphere at this NH_2trz/Fe^{2+} ratio is essentially occupied by NH_2trz ligands and does not differ significantly from that at the NH_2trz/Fe^{2+} ratio of 12/1. At an NH_2trz/Fe^{2+} ratio of around 9/1 the equilibrium is virtually completely on the side of the polymers, which are very rigid according to SAXS analysis with Fe^{2+} ions essentially in the low-spin state. A further increase of NH_2trz/Fe^{2+} ratios up to 15/1 did not lead to substantial changes of the equilibrium situation according to UV/vis spectra.

At NH_2trz/Fe^{2+} = 3/1, EXAFS analysis indicates that essentially all Fe^{2+} ions are part of polynuclear or oligonuclear complexes; however, two different Fe−Fe distances arise, at 3.31 and 3.94 Å. These are attributed to iron atoms in the low-spin and high-spin states, respectively. Such differences are remarkably large, as also observed in a similar compound (3.33 Å in the low-spin state and 3.82 Å in the high-spin state).[3] XANES and EXAFS analysis revealed that about 45% of the Fe^{2+} ions are in the high-spin state and 55% in the low-spin state at NH_2trz/Fe^{2+} = 3/1. Hence, the only compound significantly absorbing in UV/vis spectra is obviously $[Fe(NH_2trz)_3]^{2+}$ in the low-spin state, at any Fe^{2+} and NH_2trz concentration and reaction time applied here, as the signal shapes in all spectra are virtually identical (an example is given in Figure SI-10, Supporting Information). Note that entities such as $[Fe(DMF)_2(NH_2trz)_2]^{2+}$ and $[Fe(DMF)_4(NH_2trz)]^{2+}$ could be in the high-spin state and therefore not absorb significantly in UV/vis spectra. However, as the strictly mononuclear moiety $[Fe(tpz)_2]^{2+}$ with a ligand sphere similar to that of $[Fe(NH_2trz)_3]^{2+}$ is also in the low-spin state, it appears that a polynuclear structure is not a requirement for a low-spin state.

The shift of the equilibrium toward rigid-rod objects is conspicuously accompanied by a shift of the Fe^{2+} centers toward the low-spin state, and at NH_2trz/Fe^{2+} ratios of 6/1 and 12/1 only low-spin centers were found within the detection

dx.doi.org/10.1021/ic403035u | Inorg. Chem. 2014, 53, 3546−3557

limits of XANES spectroscopy: i.e., a minor fraction of high-spin states could still be present. EXAFS analysis and UV/vis spectroscopy also reveal the predominant presence of low-spin states at a NH_2trz/Fe^{2+} ratio of 12/1. It is obvious that the $[Fe(NH_2trz)_3]^{2+}$ complexes feature a distinct color in the low-spin state, while in the high-spin state $[Fe(NH_2trz)_3]^{2+}$ (and other species) are expected to be almost colorless.[30] Remarkably, all UV/vis spectra have the same shape, as illustrated by the coincidence of the band shape at NH_2trz/Fe^{2+} ratios of 3/1 and 15/1 (Figure SI-10, Supporting Information). Hence, it appears that $[Fe(NH_2trz)_3]^{2+}$ is the only low-spin species which is present in considerable quantities. As XANES data do not reveal significant differences in the spin state at NH_2trz/Fe^{2+} ratios of 6/1 and 12/1, in contrast to UV/vis spectra, it appears that the latter are somewhat more sensitive to structural changes. Maximum absorption in UV/vis spectra is observed when the linear polynuclear complexes have virtually complete rigidity according to SAXS measurements.

At the ratio NH_2trz/Fe^{2+} = 3/1 XANES reveals that 55% of the Fe^{2+} ions are in the low-spin state (c_{Fe} = 0.0185 mol L^{-1}). However, taking the UV/vis spectra at NH_2trz/Fe^{2+} of 15/1 as a reference for the low-spin state, only 33% of low-spin states is then calculated at NH_2trz/Fe^{2+} = 3/1 according to the Bouguer–Lambert–Beer law.[39−43] This difference could indicate that the extinction coefficient increases with increasing development of rigid-rod-like structures, which can originate in transition dipole moments that induce dipole moments in neighboring chromophores.[44] This would imply that the extinction coefficient (ε) increases the more the rigid polynuclear structure is established and finally reaches a value of about 35 M^{-1} cm^{-1} (at λ_{max}, ε referring to a monomer unit), which is reached at a NH_2trz/Fe^{2+} ratio of around 9/1. This extinction coefficient is indeed on the order of values of mononuclear iron(II) pyrazolylborate spincrossover complexes in the low-spin state.[30]

Heating of solutions with c_{Fe} = 0.0185 M and NH_2trz/Fe^{2+} = 9/1 to 60 °C led to a reversible color change from pink to colorless, implying a transition from low-spin to high-spin states. SAXS analysis revealed that the linear rigid-rod-like objects present at room temperature turn into smaller entities at 60 °C. Hence, spin crossover is also observed in solution, but this process is accompanied by a shift in equilibrium toward shorter species, most likely in contrast to spin crossover in the solid state. Dissociation of the polynuclear complex in solution might be favored by an enthalpic contribution to the total change in energy: in the high-spin state the metal–ligand bonds are weaker than in the low-spin state due to the occupation of antibonding orbitals by electrons in the high-spin state and therewith an increase in Fe–N bond length.

Solutions of polynuclear complexes of Fe^{2+} and NH_2trz allow the preparation of $[Fe(NH_2trz)_3](2ns)_2$ films with spincrossover behavior. The processability of SCO materials as thin films is a forefront topic of research in the SCO field. This work demonstrates for the first time that this type of SCO polymer can be processed from solution.

CONCLUSIONS

$[Fe(NH_2trz)_3]^{2+}$ is generated in DMF within minutes in a reversible process when $[Fe(DMF)_6]^{2+}$ and NH_2trz are mixed (total Fe^{2+} concentrations around 0.02 M). The polynuclear complexes thus obtained can be studied with UV/vis absorption spectroscopy, SAXS, XANES, and EXAFS. There is essentially no presence of $[Fe(NH_2trz)_3]^{2+}$ at a molar NH_2trz/Fe^{2+} ratio of 1/1 and little presence at a ratio of 2/1. Increasing the ratio to 3/1, however, leads to considerable quantities of $[Fe(NH_2trz)_3]^{2+}$. This polymer is, however, in equilibrium with shorter species, where the shorter species are also predominantly polynuclear compounds. In general, it appears that the low-spin state arises only when the NH_2trz ligand sphere is established to a high extent in polynuclear rigid-rod structures. The Fe–Fe distances and colors depend strikingly on the spin state (around 3.32 Å for the pink low-spin state and 3.94 Å for the virtually colorless high-spin state). At an NH_2trz/Fe^{2+} ratio of 9/1 the equilibrium is virtually completely shifted to the side of rodlike low-spin $[Fe(NH_2trz)_3]^{2+}$ complexes. In such solutions, reversible spin crossover is observed upon heating to 60 °C. However, this phenomenon involves not only the common expansion of Fe–N bonds but also a shift in equilibrium to the side of shorter species, most likely in contrast to spin crossover in the solid state.

Thus, since $[Fe(NH_2trz)_3]^{2+}$ exists in solution in DMF, it should be possible to process the polynuclear spincrossover complex $[Fe(NH_2trz)_3](2ns)_2$ from this solvent. In contrast, water and DMSO are not suited for this purpose due to the adverse position of the equilibria. Finally, films were prepared from DMF solution at an NH_2trz/Fe^{2+} ratio of 3/1, which show thermochromic behavior, like powders of $[Fe(NH_2trz)_3](2ns)_2$. It appears, therefore, that the spin crossover is retained upon film preparation from solution.

ASSOCIATED CONTENT

Supporting Information

Figures, tables, and a CIF file giving UV/vis absorption spectra and color pictures of $[Fe(H_2O)_6]^{2+}/NH_2trz$ solutions in the presence and absence of ascorbic acid, information on the crystal structure of $[Fe(tpz)_2](2ns)_2 \cdot 2MeOH$, experimental and calculated scattering data of polymers, and experimental and calculated EXAFS spectra. This material is available free of charge via the Internet at http://pubs.acs.org. Crystallographic data for the reported structure have also been deposited with the Cambridge Crystallographic Data Centre under no. CCDC-965587. They can be obtained free of charge from The Cambridge Crystallographic Data Centre via http://www.ccdc.cam.ac.uk/Community/Requestastructure/.

AUTHOR INFORMATION

Corresponding Author

*E-mail for W.C.: wcaseri@mat.ethz.ch.

Notes

The authors declare no competing financial interest.

ACKNOWLEDGMENTS

We express our deep gratitude to Paul Smith for helpful discussions and valuable advice concerning the present paper. We are also very grateful to the responsible scientist Dr. Edmund Welter at beamline A1, Hasylab (Hamburg, Germany) and to Dr. Alexander Pöthig (Technische Universität München) for helpful discussions. The financial support of the Swiss National Science Foundation (No. 200021_137550) is acknowledged.

REFERENCES

(1) Roubeau, O. *Chem. Eur. J.* **2012**, *18*, 15230–15244.

(2) Grosjean, A.; Daro, N.; Kauffmann, B.; Kaiba, A.; Létard, J.-F.; Guionneau, P. *Chem. Commun.* **2011**, *47*, 12382−12384.
(3) Yokoyama, T.; Murakami, Y.; Kiguchi, M.; Komatsu, T.; Kojima, N. *Phys. Rev. B* **1998**, *58*, 14238−14244.
(4) Michalowicz, A.; Moscovici, J.; Ducourant, B.; Cracco, D.; Kahn, O. *Chem. Mater.* **1995**, *7*, 1833−1842.
(5) Smit, E.; de Waal, D.; Heyns, A. M. *Mater. Res. Bull.* **2000**, *35*, 1697−1707.
(6) Real, J. A.; Gaspar, A. B.; Muñoz, M. C. *Dalton Trans.* **2005**, 2062−2079.
(7) Armand, F.; Badoux, C.; Bonville, P.; Ruaudel-Teixier, A.; Kahn, O. *Langmuir* **1995**, *11*, 3467−3472.
(8) Postema, A. R.; Liou, K.; Wudl, F.; Smith, P. *Macromolecules* **1990**, *23*, 1842−1845.
(9) Dîrtu, M. M.; Garcia, Y.; Nica, M.; Rotaru, A.; Linares, J.; Varret, F. *Polyhedron* **2007**, *26*, 2259−2263.
(10) Lavrenova, L. G.; Shakirova, O. G.; Ikorskii, V. N.; Varnek, V. A.; Sheludyakova, L. A.; Larionov, S. V. *Russ. J. Coord. Chem.* **2003**, *29*, 22−27; *Koord. Khim.* **2003**, *29*, 24−30.
(11) van Koningsbruggen, P. J.; Garcia, Y.; Codjovi, E.; Lapouyade, R.; Kahn, O.; Fournès, L.; Rabardel, L. *J. Mater. Chem.* **1997**, *7*, 2069−2075.
(12) Dîrtu, M. M.; Neuhausen, C.; Naik, A. D.; Rotaru, A.; Spinu, L.; Garcia, Y. *Inorg. Chem.* **2010**, *49*, 5723−5736.
(13) Reger, D. L.; Grattan, T. C.; Brown, K. J.; Little, C. A.; Lamba, J. J. S.; Rheingold, A. L.; Sommer, R. D. *J. Org. Chem.* **2000**, *607*, 120−128.
(14) Lu, K.-q.; Stern, E. A. *Nucl. Instrum. Methods* **1983**, *212*, 475−478.
(15) Bauer, M.; Heusel, G.; Mangold, S.; Bertagnolli, H. *J. Synchrotron Radiat.* **2010**, *17*, 273−279.
(16) Bauer, M.; Gastl, C. *Phys. Chem. Chem. Phys.* **2010**, *12*, 5575−5584.
(17) Binsted, N.; Hasnain, S. S. *J. Synchrotron Radiat.* **1996**, *3*, 185−196.
(18) *CrysAlis CCD and CrysAlis RED, Version 1.171.34.49*, Oxford Diffraction Ltd, Abingdon, Oxfordshire, U.K., 2011.
(19) Sheldrick, G. M. *Acta Crystallogr.. Sect. A* **2008**, *64*, 112−122.
(20) Hübschle, C. B.; Sheldrick, G. M.; Dittrich, B. *J. Appl. Crystallogr.* **2011**, *44*, 1281−1284.
(21) *CrystalMaker*; CrystalMaker Software Ltd, Oxford, U.K.
(22) Lavrenova, L. G.; Yudina, N. G.; Ikorskii, V. N.; Varnek, V. A.; Oglezneva, I. M.; Larionov, S. V. *Polyhedron* **1995**, *14*, 1333−1337.
(23) Khan, M. M. T.; Martell, A. E. *J. Am. Chem. Soc.* **1967**, *89*, 4176−4185.
(24) Muneta, P.; Kaisaki, F. *American Potato Journal* **1985**, *62*, 531−536.
(25) Vankó, G.; Neisius, T.; Molnár, G.; Renz, F.; Kárpáti, S.; Shukla, A.; de Groot, F. M. F. *J. Phys. Chem. B* **2006**, *110*, 11647−11653.
(26) Krause, M. O.; Oliver, J. H. *J. Phys. Chem. Ref. Data* **1979**, *8*, 329−338.
(27) Bausk, N. V.; Erenburg, S. B.; Mazalov, L. N.; Lavrenova, L. G.; Ikorskii, V. N. *J. Struct. Chem. (THEOCHEM)* **1994**, *35*, 509−517.
(28) Bauer, M.; Kauf, T.; Christoffers, J.; Bertagnolli, H. *Phys. Chem. Chem. Phys.* **2005**, *7*, 2664−2670.
(29) Bauer, M.; Gastl, C.; Köppl, C.; Kickelbick, G.; Bertagnolli, H. *Monatsh. Chem.* **2006**, *137*, 567−581.
(30) Jesson, J. P.; Trofimenko, S.; Eaton, D. R. *J. Am. Chem. Soc.* **1967**, *89*, 3158−3164.
(31) Baumgartner, O. *Z. Kristallogr.* **1986**, *174*, 253−263.
(32) Linert, W.; Gutmann, V.; Baumgartner, O.; Wiesinger, G.; Kirchmayr, H. *Inorg. Chim. Acta* **1983**, *74*, 123−130.
(33) Young, A. C. M.; Walters, M. A.; Dewan, J. C. *Acta Crystallogr., Sect. C* **1989**, *45*, 1733−1736.
(34) Lode, C.; Krautscheid, H. *Z. Anorg. Allg. Chem.* **2000**, *626*, 326−331.
(35) Albinati, A.; Calderazzo, F.; Marchetti, F.; Mason, S. A.; Melai, B.; Pampaloni, G.; Rizzato, S. *Inorg. Chem. Commun.* **2007**, *10*, 902−905.
(36) Li, Y.; Zhang, Z.-X.; Li, K.-C.; Song, W.-D.; Cui, X.-B.; Pan, L.-Y. *J. Mol. Struct. (THEOCHEM)* **2007**, *843*, 102−106.
(37) Stieler, R.; Bublitz, F.; Lang, E. S.; de Oliveira, G. M. *Polyhedron* **2012**, *35*, 137−141.
(38) Nitschke, C.; Köckerling, M. *Inorg. Chem.* **2011**, *50*, 4313−4321.
(39) Bouguer (initials not indicated in the original article) *Essai d'optique sur la gradation de la lumiere*; Claude Jombert: Paris, 1729.
(40) Bouguer (initials not indicated in the original article) *Traité d'optique sur la gradation de la lumiere, ouvrage postume de M. Bouguer*; Ed. l'Abbé de la Caille, H. L. Guerin & L. F. Delatour: Paris, 1760.
(41) Lambert, I. H. *Photometria sive de Mensura et Gradibus Lumnis, Colorum et Umbrae*; Eberhardt Klett: Augusta Vindelicorum (Augsburg), Germany, 1760.
(42) Lambert (initials not indicated in the original article) *Lambert's Photometrie (Photometria sive de mensura et gradibus luminis, colorum et umbrae) (1760), Erstes Heft: Theil I und II*; Anding, E., Ed.; Wilhelm Engelmann: Leipzig, Germany, 1892.
(43) Beer (initials not indicated in the original article) *Pogg. Ann.* **1852**, *86* (5), 78−88. Beer *Ann. Phys. Chem.* **1852**, *163* (5), 78−88.
(44) Schmidt, W. *Optische Spektroskopie*; Wiley-VCH: Weinheim, Germany, 2000.